SLAC–PUB–3435
September 1984
(T/E)

THE J/ψ DECAYS INTO A VECTOR AND A PSEUDOSCALAR MESON AND THE QUARK CONTENT OF THE η AND η' *

The MARK III Collaboration

R.M. Baltrusaitis,[a] D. Coffman, J. Hauser, D.G. Hitlin,
J.D. Richman,[b] J.J. Russell,[c] and R.H. Schindler
California Institute of Technology, Pasadena, CA 91125

D.E. Dorfan, R. Fabrizio,[d] F. Grancagnolo,[b] R.P. Hamilton,[e]
C.A. Heusch, L. Köpke, R. Partridge, J. Perrier, H.F.W. Sadrozinski,
M. Scarlatella, T.L. Schalk, and A. Seiden
University of California at Santa Cruz, Santa Cruz, CA 95064

J.J. Becker,[f] G.T. Blaylock, J.S. Brown, H. Cui,[g]
B.I. Eisenstein, G. Gladding, S.A. Plaetzer, A.L. Spadafora,[h]
J.J. Thaler, A. Wattenberg, and W.J. Wisniewski
University of Illinois at Urbana-Champaign, Urbana, IL 61801

K.O. Bunnell, R.E. Cassell, D.H. Coward, K.F. Einsweiler,[b]
L. Moss, R.F. Mozley, A. Odian, J.R. Roehrig,[i] W. Toki,
Y. Unno,[j] F. Villa, N. Wermes, and D. Wisinski
Stanford Linear Accelerator Center, Stanford, CA 94305

T.H. Burnett, V. Cook, C. Del Papa,[b] A.L. Duncan,
P.M. Mockett, A. Nappi,[k] J.C. Sleeman,[l] and H.J. Willutzki
University of Washington, Seattle, WA 98195

Submitted to Physical Review D

---

* Work supported in part by the Department of Energy, contract numbers DE – AC03-76SF00515, DE – AC02-76ER01195, DE – AC03-81ER40050, DE – AM03-76SF00034, and by the National Science Foundation.

ABSTRACT

From a study of 2.7 million J/ψ decays with the Mark III detector at SPEAR, we have obtained new measurements of the two body decays of the J/ψ into a vector and a pseudoscalar meson. We present branching ratios for decays to: $\rho\pi$, $KK^*(892)$, $\phi\eta$, the previously unobserved modes $\phi\eta\prime$, $\omega\eta$, $\omega\eta\prime$, $\omega\pi^0$, $\rho^0\eta$, and new upper limits on $\rho^0\eta\prime$ and $\phi\pi^0$. In the decay $J/\psi \to \eta\pi^+\pi^-$, we observe $\rho^0 - \omega$ interference. The collection of measured branching ratios are simultaneously fit to a simple model of J/ψ decays which includes strong and electromagnetic amplitudes and allows for violation of SU(3) invariance. Using this model, we calculate the strange and non-strange quark content of the η and $\eta\prime$ and conclude that $(35 \pm 18)\%$ of the $\eta\prime$ wave function can be attributed to an additional component, e.g. gluonium or radial excitation. The measurement of the $\omega\pi^0$ branching ratio, when combined with that of the $\gamma\pi^0$ decay mode of the ω, yields a determination of the $\omega\pi^0$ electromagnetic form factor ratio $|f(q^2 = m^2_{J/\psi})/f(q^2 = 0)| = 0.038 \pm 0.006$.

1. Introduction

The J/ψ provides a unique system for the study of hadron dynamics. It is a system with well defined initial quantum numbers, devoid of u, d, or s quarks, and with sizeable branching fractions into simple modes. Fig. 1 shows the four diagrams believed to be mainly responsible for the decay of the J/ψ. These are:

1. Three gluon annihilation into hadrons.

2. Electromagnetic decay proceeding via a single virtual photon. This process yields e^+e^- and $\mu^+\mu^-$ pairs as well as hadrons.

3. Radiative decay into a real photon and two gluons.

4. Magnetic dipole radiative transition to the $\eta_c(2980)$.

The relative rates for these processes are predicted to be $67 : 23 : 8 : 2$.[1]

This paper reports on the two body decays of the J/ψ into a vector meson, V (K^*, ρ, ω, or ϕ), plus a pseudoscalar meson, P (K, π, η, or $\eta\prime$). The decays to the VP pairs are expected to occur through the 3–gluon or the electromagnetic diagrams. Several authors[2] have pointed out that glueball and radially excited quark-antiquark states could mix with mesons with the same quantum numbers, and that the values of the $J/\psi \rightarrow VP$ branching ratios can be used to determine the strange and non-strange quark content of the pseudoscalar mesons as well as possible additional components. The rate of the $J/\psi \rightarrow \omega\pi^0$ decay can be related to the $\omega \rightarrow \gamma\pi^0$ decay rate via an electromagnetic form factor if single photon annihilation is the only process involved.

Section II of this paper concerns the experimental details of the analysis and determination of branching ratios. In Section III, we discuss interpretations of the data, including evaluation of the quark content of the pseudoscalar mesons[2,3] and determination of electromagnetic form factors.

2. Details of the Analysis

The Mark III spectrometer is a general purpose magnetic detector designed for detailed studies of exclusive final states in the SPEAR energy region. The detector is described in detail elsewhere.[4] We limit ourselves here to a brief survey of the relevant features. The axial and transverse views of the detector are shown in Fig. 2. A low mass inner drift chamber surrounding the beryllium beam pipe provides tracking and a first level trigger. The main drift chamber system, in a 0.4 T magnetic field, measures the momentum of charged tracks over 84% of the solid angle with a resolution of $\sigma_p/p = 0.015\sqrt{1+p^2}$ (p in GeV/c). Two stereo layers and charge division on four of the axial layers provide a measure of the dip angle. Charged particle identification is obtained with a system of 48 time–of–flight (TOF) counters. These counters, which cover 80% of the solid angle, have a time resolution σ_t of 190 psec for hadrons. This provides 3σ π/K separation for momenta up to 800 MeV/c.

Between the TOF counters and the solenoid coil is a highly segmented gas sampling calorimeter consisting of 24 layers of alternating proportional counters and 1/2 radiation length lead sheets. Endcap shower counters of similar design extend the photon detection capability to 94% of the solid angle. The shower counters measure photon angles with a resolution σ_θ of 10 mrad and photon energies with a resolution σ_E/E of $0.17/\sqrt{E}$ (E in GeV). The shower counter is fully efficient for photon energies greater than 100 MeV; this feature is crucial for the reconstruction of final states which have several photons.

Before discussing the analyses of the various specific decay modes, we note some common features. In general, the analysis of a given state begins with all events having the correct topology for the state (exact number of charged tracks and a number of showers equal or larger than that required by the final state). The TOF

system is used to distinguish kaons from pions whenever possible. The identification of photons is complicated by the fact that charged particles often interact in the shower counters, producing clusters of hits ("split-offs") which can be mistaken for photon signals. The confusion is minimized by eliminating all photons for which the angle between the shower and the nearest charged track is less than 18° or by using only the highest energy showers. When the number of showers is larger than that expected for the final state, the energy of each additional shower is required to be small (usually less than 60 MeV).

The events are kinematically fit by imposing energy, momentum, and any relevant mass constraints. This fit substantially improves the photon energy resolution, which in turn improves the determination of the invariant masses of subgroups of particles in the final state. After fitting, the mass resolution is typically 1%. In addition, the fits help in the reconstruction of events with spurious photons. In such events, all photon combinations are tried in the fit and the confidence level is used to identify the most probable set of photons.

The yield for a specific decay mode is determined from resonant peaks in the invariant mass distributions. Signal yields are extracted using a maximum likelihood fit of the appropriate Breit–Wigner shapes, folded with the resolution, and a polynomial for the background. To study the background, mass sidebands surrounding the resonance are selected.

The detection efficiency for a specific decay mode is estimated by generating events of the desired type by Monte Carlo and passing them through the entire analysis chain. For the decay $J/\psi \to VP$, the matrix element in the J/ψ rest frame is proportional to $\hat{e}_{J/\psi} \cdot \hat{e}_V \times \vec{P}_V$,[5] where $\hat{e}_{J/\psi}$ and $\hat{e}_V$ are the respective polarization vectors, and $\vec{P}_V$ is the momentum of the vector meson. With the known decay amplitudes for the pseudoscalar and vector mesons, all the angular distributions are completely determined; the only unknown is the strength of the amplitude. Knowl-

edge of the angular distributions is necessary to correctly simulate the detection efficiency and also provides a check of the observed distributions.

The angular distribution of the decay sequence $J/\psi \to VP$, $V \to PP$ or PPP is described by

$$\frac{d^3\sigma}{d\cos\theta_V\, d\cos\theta_1\, d\varphi_1} = \sin^2\theta_1 \left[1 + \cos^2\theta_V + \sin^2\theta_V \cos(2\varphi_1)\right], \qquad (1)$$

where θ_V is the angle between the vector meson and the positron direction and θ_1 and φ_1 describe the decay products of the vector meson in its helicity frame. For the two body decays, such as $\rho^0 \to \pi^+\pi^-$ and $\phi \to K^+K^-$, θ_1 and φ_1 are the polar and azimuthal angles of the momentum of the $\pi(K)$ with respect to the helicity direction of the $\rho^0(\phi)$. For the three body decay $\omega \to \pi^+\pi^-\pi^0$, θ_1 and φ_1 are the angles between the normal to the decay plane and the helicity direction. To fully describe the final state, the isotropic distribution from the decay of the pseudoscalar meson needs to be combined with Eqn. (1).

We now turn to a discussion of the details of the analysis specific to each channel. Table 1 gives the branching ratios we have obtained from our sample of 2.7 million produced J/ψ's. The statistical and systematic errors pertaining to each specific mode are given. The major contribution ($\approx$ 10%) to the systematic error comes from uncertainties in the Monte Carlo simulation. An overall systematic error of 5.8% arises from the determination of the total number of produced J/ψ.[6]

2.1 $\rho\pi$ AND K^*K

The Dalitz plots of Fig. 3 show that the $\pi^+\pi^-\pi^0$, $K^+K^-\pi^0$, and $K^0_S K^\pm\pi^\mp$ final states are almost entirely dominated by $\rho\pi$ and K^*K, respectively. Dividing each Dalitz plot into three parts, corresponding to the bands of the triangular regions, one finds that the number of events in each charge combination can be determined with almost no background. As a check, the ratio $\rho^0\pi^0/\rho^\pm\pi^\mp = 0.50 \pm 0.04$ agrees

well with the value of 0.5 expected from isospin symmetry. The $K^{*\pm}K^{\mp}$ rate can be determined either from the decay mode $K^{\pm}\pi^{\mp}K^0_S$, where the K_S is identified by its $\pi^+\pi^-$ decay, or from the decay to $K^+K^-\pi^0$. Within the quoted errors, which are predominantly systematic, the rates are consistent with each other.

2.2 $\omega\pi^0$ AND $\omega\eta$

Both of these decay modes are observed in the topology $\pi^+\pi^-\gamma\gamma\gamma\gamma$. Looking at all combinations and selecting events having a $\pi^+\pi^-\pi^0$ mass compatible with an ω, we examine the momentum and mass spectra for the remaining two photons,[7] which are shown in Fig. 4. The recoil momentum spectrum, when fitted with two Breit–Wigner shapes, folded with a Gaussian to take into account the momentum resolution, plus a linear background, gives the number of $\omega\pi^0$ and $\omega\eta$ events. The distribution of $\cos\theta_1$, the cosine of the angle between the normal to the decay plane and the helicity direction of the ω, is shown in Fig. 5. The data agree well with the $\sin^2\theta$ distribution (Eqn. (1)) expected for an ω having helicity ±1 only, as required for this decay.

2.3 $\phi\eta$ AND $\phi\pi^0$

These events are observed in the topology $K^+K^-\gamma\gamma$. Since the kaons from ϕ decays are relatively soft (< 800 MeV/c), they are easily distinguished from pions by the TOF system. Requiring both K's to be identified by the TOF gives a very clean ϕ signal.[8] The $J/\psi \to \phi\eta$ decays produce a peak centered at 1.32 GeV/c in the momentum spectrum of ϕ's recoiling against neutral tracks. A fit to a Gaussian and a polynomial yields the first branching ratio given in Table 1. Evidence for the $\phi\eta$ channel is also given by the prominent peak at 0.55 GeV/c in the $\gamma\gamma$ invariant mass spectrum for events satisfying a 4C fit to $\gamma\gamma K^+K^-$ (Fig. 6). There is, however, no signal corresponding to the OZI violating[9] decay $J/\psi \to \phi\pi^0$. The 90% confidence level upper limit on this branching ratio is given in Table 1.

The decay $J/\psi \to \phi\eta$ is also observed with the η decaying to $\pi^+\pi^-\pi^0$. This channel appears in the $J/\psi \to K^+K^-\pi^+\pi^-\pi^0$ topology discussed in the next section.

2.4 $\phi\eta\prime$ AND $\omega\eta\prime$

For these measurements, we identify the $\eta\prime$ both by its decay

$$\eta\prime \to \gamma\,\rho^0 \qquad \rho^0 \to \pi^+\pi^- \tag{2}$$

and its decay

$$\eta\prime \to \pi^+\pi^-\eta \qquad \eta \to \gamma\gamma \tag{3}$$

The ϕ and ω are identified by their K^+K^- and $\pi^+\pi^-\pi^0$ decay modes, respectively. Thus these states appear in the data as events with four charged tracks and one or more photons.

The K^+K^- invariant mass from our four prong sample is shown in Fig. 7a. When fit to a Gaussian and a polynomial background, this distribution yields a ϕ mass equal to (1.0194 ± 0.0003) GeV/c^2 and a resolution $\sigma = (4.5 \pm 0.3)$ MeV/c^2. For events containing a ϕ and satisfying a 4C fit to the hypothesis $J/\psi \to \gamma\pi^+\pi^-K^+K^-$, the $\pi^+\pi^-$ invariant mass is plotted versus the $\pi^+\pi^-\gamma$ mass in Fig. 7b. Evidence for the decay (2) is given by the cluster of events with a $\pi^+\pi^-$ mass consistent with a ρ^0 and a $\gamma\pi^+\pi^-$ mass consistent with that of the $\eta\prime$.

The analysis of the decay $J/\psi \to \phi\eta\prime$ where the $\eta\prime$ decays via Eqn. (3) proceeds in a similar manner, but requires one additional photon. For events satisfying a 4C fit to the hypothesis $J/\psi \to \gamma\gamma\pi^+\pi^-K^+K^-$, and containing a ϕ, the $\gamma\gamma$ invariant mass is plotted versus the $\gamma\gamma\pi^+\pi^-$ mass in Fig. 7c. A cluster of events which corresponds to the decay $J/\psi \to \phi\eta\prime$ can be seen, where the $\eta\prime$ decays into

$\eta\pi^+\pi^-$. This scatter plot also shows evidence for the decay chain $J/\psi \to \phi\eta$, $\eta \to \pi^+\pi^-\pi^0$, $\pi^0 \to \gamma\gamma$ discussed in the previous section.

In the Monte Carlo calculation of the efficiency, a phase space model is used for the decay $\eta\prime \to \eta\pi^+\pi^-$. For the sequential decay $\eta\prime \to \gamma\rho^0$, $\rho^0 \to \pi^+\pi^-$, the Breit-Wigner shape of the ρ^0, the appropriate two body phase space, and the E_γ dependence of the magnetic dipole transition are taken into account.

The $\omega\eta\prime$ decay is somewhat more complicated because of the combinations involved with the four pions and three or four photons. For the $\eta\prime \to \gamma\rho^0$ channel, events are required to be compatible with the hypothesis $J/\psi \to \gamma\pi^0\pi^+\pi^-\pi^+\pi^-$, $\pi^0 \to \gamma\gamma$. The three highest energy showers are used. Only 4% of the events have more than one acceptable pairing for the π^0 ($\gamma\gamma$ effective mass within $3\sigma = 34$ MeV/c^2 of that of the π^0). The $\gamma\pi^+\pi^-$ invariant mass is shown in Fig. 8a for all combinations where the recoiling $\pi^0\pi^+\pi^-$ mass is within 3σ (41 MeV/c^2) of the ω mass. The excesses of events at the mass of the η and $\eta\prime$ correspond to the decays $J/\psi \to \omega\eta$ and $J/\psi \to \omega\eta\prime$, respectively. The mass resolution obtained from the Monte Carlo simulation is 7.5 MeV/c^2 for the η and 13.5 MeV/c^2 for the $\eta\prime$. Two decay sequences contribute to the structure in the mass region of the η. The decays $J/\psi \to \omega\eta$, $\eta \to \gamma\pi^+\pi^-$ produce a peak centered at (0.550 ± 0.002) GeV/c^2 with $\sigma = (7 \pm 3)$ MeV/c^2, in very good agreement with the value expected from the Monte Carlo simulation. The expected number of background events from the decay $J/\psi \to \omega\eta$, $\eta \to \pi^0\pi^+\pi^-$ in which one of the two photons produced in the decay of the η is not detected is in agreement with the number of events and the mass distribution observed below 0.52 GeV/c^2. Although all $\gamma\pi^+\pi^-$ combinations are allowed in the mass distribution, none of the events contributes more than once. The measured $J/\psi \to \omega\eta$ branching ratios, $(1.8 \pm 0.5 \pm 0.2) \times 10^{-3}$ for the $\eta \to \gamma\pi^+\pi^-$ channel and $(1.8 \pm 0.8 \pm 0.4) \times 10^{-3}$ for $\eta \to \pi^0\pi^+\pi^-$, are in very good agreement with the value $(1.9 \pm 0.2 \pm 0.3) \times 10^{-3}$ obtained in Section 2.2. Since

the final states for the decays $J/\psi \to \omega\eta$, $\eta \to \gamma\pi^+\pi^-$ and $J/\psi \to \omega\eta\prime$, $\eta\prime \to \gamma\rho^0$ are identical, these two determinations of the $J/\psi \to \omega\eta$ branching ratio provide a useful check of the $J/\psi \to \omega\eta\prime$ analysis.

A similar analysis in which the $\eta\prime$ is observed in the $\eta\prime \to \eta\pi^+\pi^-$ channel provides another check of the $J/\psi \to \omega\eta\prime$ branching ratio measurement. Events compatible with the $\gamma\gamma\gamma\gamma\pi^+\pi^-\pi^+\pi^-$ hypothesis are subjected to a 6C fit to the hypothesis $\pi^0\eta\pi^+\pi^-\pi^+\pi^-$. There are six possible photon pairings. Because 20% of the events have more than one good pairing (χ^2-probability of the fit greater than 5%), the combinations which give the two best 6C fits are kept. In a search for $\omega\eta\prime$, there are four possible combinations of charged pions. The good mass resolution after the fit, when combined with the narrow width of the ω, allows a good selection of events: the fraction of events having more than one ω candidate ($\pi^+\pi^-\pi^0$ effective mass within 3σ = 34 MeV/c^2 of that of the ω) is 23%. The $\eta\pi^+\pi^-$ mass recoiling against the ω is shown in Fig. 8b. The ω sidebands allow a check that the $\eta\prime$ signal (5 events) does not come from the background.

2.5 $\rho^0\eta$ AND $\rho^0\eta'$

The $\rho^0\eta$ and $\rho^0\eta\prime$ final states, like $\omega\pi^0$, have isospin one; therefore these decays are electromagnetic in origin. The final state selection is relatively straight forward, especially for $\rho^0\eta$ seen in the $\gamma\gamma\pi^+\pi^-$ channel. The principal complication in the analysis occurs because of the presence of the much larger $\omega\eta$ channel. The $\omega \to \pi^+\pi^-$ branching ratio is 1.4%. Therefore interference may exist between the two channels, $J/\psi \to \rho^0\eta$, $\rho^0 \to \pi^+\pi^-$ and $J/\psi \to \omega\eta$, $\omega \to \pi^+\pi^-$.

The final state $\pi^+\pi^-\eta$ is selected by making a 4C fit to the $\gamma\gamma\pi^+\pi^-$ channel and by requiring a $\gamma\gamma$ effictive mass within 3σ = 30 MeV/c^2 of the η mass. The resulting $\pi^+\pi^-$ mass plot is shown in Fig. 9. The number of $\omega\eta$ and $\rho^0\eta$ events,

N_ω and N_{ρ^0}, are the results of a fit to the $\pi^+\pi^-$ mass distribution of the function

$$N(m_{\pi^+\pi^-}) = LinearBackground(m_{\pi^+\pi^-}) + |A_{\rho^0}(m_{\pi^+\pi^-}) + A_\omega(m_{\pi^+\pi^-}) \times e^{i\phi}|^2,$$

where $A_{\rho^0}(m_{\pi^+\pi^-})$ is the contribution of the $J/\psi \to \rho^0\eta$ channel to the amplitude, which is given by $\sqrt{N_{\rho^0}} \times BW_{\rho^0}(m_{\pi^+\pi^-})$. The Breit-Wigner amplitude† $BW_{\rho^0}(m_{\pi^+\pi^-})$ describes the ρ^0 shape. Similarly, for the $J/\psi \to \omega\eta$ channel, $A_\omega(m_{\pi^+\pi^-}) = \sqrt{N_\omega} \times BW_\omega(m_{\pi^+\pi^-})$. The relative phase, ϕ, between the two amplitudes, A_{ρ^0} and A_ω, has to be determined.

Before discussing the result, note that because $\Gamma_\omega \ll \Gamma_\rho$ and $m_\omega \simeq m_\rho$, the total number of events N_T in the ρ^0–ω mass region (background events excluded) is

$$\begin{aligned} N_T &= N_{\rho^0} + N_\omega + 2\sqrt{\frac{\Gamma_\omega}{\Gamma_\rho} N_{\rho^0} N_\omega}\ \cos\phi \\ &= N_{\rho^0} + N_\omega + 0.507\sqrt{N_{\rho^0} N_\omega}\ \cos\phi. \end{aligned}$$

Using the results from the previous section, we expect that the number of $J/\psi \to \omega\eta$, $\omega \to \pi^+\pi^-$ decays be $N_\omega = N_{J/\psi} \times B(J/\psi \to \omega\eta) \times B(\omega \to \pi^+\pi^-) \times \epsilon = (8.9 \pm 2.4)$, where ϵ is the global detection efficiency and $N_{J/\psi}$ is the total number of produced J/ψ. The number of $J/\psi \to \rho^0\eta$ decays can be estimated, as discussed in Section 3, as

$$N_{\rho^0} = N_{J/\psi} \times B(J/\psi \to \omega\pi^0) \frac{B(J/\psi \to \omega\eta)}{B(J/\psi \to \rho^0\pi^0)} \times \epsilon = 96 \pm 30.$$

Since N_{ρ^0} is expected to be about ten times bigger than N_ω, the interference term can make a larger contribution to the total number of events than the term given

---

† $BW(s = m^2_{\pi^+\pi^-}) = \sqrt{\frac{\Gamma(s)\cdot m}{\pi}} \frac{1}{m^2 - s - i\Gamma(s)\cdot m}$ where m is the mass of the resonance. The width Γ varies with energy and is given by $\Gamma(s) = \Gamma_0 \left(\frac{P^*}{P_0^*}\right)^3 \frac{2P_0^*}{P_0^{*2} + P^{*2}}$ where Γ_0 is the width at $\sqrt{s} = m$; P_0^* and P^* are the momenta of the pions in the resonance center of mass at $\sqrt{s} = m$ and $m_{\pi^+\pi^-}$, respectively.[10]

by N_ω. The numbers of $J/\psi \to \rho^0\eta$ and $J/\psi \to \omega\eta$ events determined from the fit (Table 2) are in good agreement with the previous estimates. The interference term contributes $\approx 20\%$ of the total decay rate (15 events).

The $\rho^0\eta\prime$ channel is searched for in the final state $\gamma\gamma\pi^+\pi^-\pi^+\pi^-$ where the $\eta\prime$ is identified by its $\eta\pi^+\pi^-$ decay. No signal is observed and an upper limit with a 90% confidence level is given in Table 1.

3. Interpretation of Results

3.1 Decays involving η and $\eta\prime$

The OZI–suppressed[9] decay of the J/ψ into three gluons results in a hadronic width which is very much smaller than widths typical of decays of the lighter vector mesons. Aside from the OZI suppression common to all hadronic J/ψ decays, the contribution of doubly disconnected diagrams, like the one shown in Fig. 10a where an $s\bar{s}$ recoils against a non-strange pair, is suppressed relative to that of singly disconnected diagrams (Fig. 10b) by an additional OZI suppression factor. We expect therefore to observe the decays $J/\psi \to \omega f$ and $J/\psi \to \phi f'$ but not $J/\psi \to \omega f'$ or $J/\psi \to \phi f$, the tensor mesons being approximately ideally mixed. This is, indeed, the experimental situation.[11] The suppression of the disconnected diagrams results in a much smaller branching ratio for $\phi\pi^0$ than for $\omega\pi^0$ as seen in our data. Thus, for two body final states, the OZI rule completely correlates the quark flavors in the two states. Since the quark content of the vector mesons is reasonably well established, $J/\psi \to VP$ decays can be used to probe the quark content of the pseudoscalar mesons.

The masses and mixing angles of the η and $\eta\prime$ mesons have been a long–standing problem. Recently there have been attempts to understand this problem by allowing these states to mix with a hypothesized pseudoscalar state composed of gluons.[2,12]

In Rosner's formulation[2], the meson wave functions can be written

$$|\eta\rangle = X_\eta|N\rangle + Y_\eta|S\rangle + Z_\eta|G\rangle$$
$$|\eta\prime\rangle = X_{\eta\prime}|N\rangle + Y_{\eta\prime}|S\rangle + Z_{\eta\prime}|G\rangle$$

where the basis states are

$$|N\rangle = \frac{|u\bar{u} + d\bar{d}\rangle}{\sqrt{2}}, |S\rangle = |s\bar{s}\rangle, |G\rangle = |Gluonium\rangle,$$

with normalisation

$$X^2 + Y^2 + Z^2 = 1,$$

for the η and $\eta\prime$ separately. If $Z_\eta = Z_{\eta\prime} = 0$, the X's and Y's are directly related to the traditional pseudoscalar mixing angle.

The width of the decay $J/\psi \to VP$ is given by[11]

$$\Gamma(J/\psi \to VP) = \frac{1}{32\pi^2\, m_{J/\psi}} \times \left(\frac{P_V}{m_{J/\psi}}\right) \times \sum_{spins} \int |\mathcal{M}|^2 d\Omega_V \qquad (4)$$

with $\mathcal{M} = g_{VP}\, m_{J/\psi}\, \hat{e}_{J/\psi} \cdot \hat{e}_V \times \vec{P}_V$ (see Section 2). In Eqn. (4) , only two quantities depend on the particular VP final state: the center of mass momentum P_V and the constant g_{VP}. We factor out the P_V dependence and write the branching ratio as

$$B(J/\psi \to VP) = |\mathrm{A}|^2 \times P_V^3,$$

with A = Constant $\times\, g_{VP}$. The amplitude A, which has contributions from both the three gluon diagram and the one photon diagram, can be expressed in terms of an SU(3) symmetric strong amplitude (g) and an electromagnetic amplitude (e).[13] Their contributions to a specific channel are obtained through a standard SU(3) calculation (see Appendix) which yields the result shown in Table 3. SU(3) violation has been taken into account by a pure octet SU(3) breaking term. This is equivalent to reducing g by a fixed amount h for each strange quark in the final state and to

multiplying the electromagnetic amplitude contributions, which are proportional to the quark magnetic moment μ, by different functions of $x = \frac{\mu_s}{\mu_u} \simeq \frac{m_u}{m_s}$, where m_s and m_u are the strange and non-strange quark masses.

Because the $J/\psi \to \rho^0\pi^0$ and $J/\psi \to \omega\eta$ amplitudes are identical up to a coefficient X_η, after correction for the P_V^3 factors, the ratio of their branching ratios is[14]

$$\frac{B(J/\psi \to \omega\eta)}{B(J/\psi \to \rho^0\pi^0)} = X_\eta^2. \tag{5}$$

Similarly,

$$\frac{B(J/\psi \to \rho^0\eta)}{B(J/\psi \to \omega\pi^0)} = X_\eta^2. \tag{6}$$

The values of X_η^2, $X_{\eta'}^2$ and $Y_\eta^2/Y_{\eta'}^2$ derived from (5) and (6) and similar equations are given in Table 4. An overall systematic error of 5.8%, arising from the determination of the total number of produced J/ψ, common to all the branching ratios, is not taken into account in this calculation since it does not affect the result of the analysis. The X^2 values obtained from the 3-gluon annihilation dominated decays, $\rho^0\pi^0$, $\omega\eta$, and $\omega\eta'$, are in agreement (within 1.4σ) with those obtained from the purely electromagnetic decays, $\omega\pi^0$, $\rho^0\eta$, and $\rho^0\eta'$.

Fitting the measured branching ratios with the set of amplitudes given in Table 3, we can determine all of the parameters: $|g|$, $|h|$, $|e|$, ϕ(relative phase between (g, h) and e), the X's, and the Y's. An average value is used for each branching ratio that is measured in more than one final state. The result of the global fit is given in Table 5 and presented in Fig. 11a and Fig. 11b. The χ^2–probability of the fit is 14%. The parameter $x = \frac{\mu_s}{\mu_u}$ was fixed at 0.62.[15] A 15% change in x affects the results by less than 4%. Note that the measured SU(3) breaking $|h|/|g|$ is equal to $(21 \pm 6)\%$, that the relative contribution of the single photon and 3-gluon annihilation diagrams is $|e|/|g| \simeq (13 \pm 1)\%$, and that the phase $\phi = 1.19 \pm 0.20$ is

close to $\pi/2$. Adding the non-strange and strange quark contents, we get

$$X_\eta^2 + Y_\eta^2 = 1.1 \pm 0.2$$
$$X_{\eta\prime}^2 + Y_{\eta\prime}^2 = 0.65 \pm 0.18. \tag{7}$$

The X's and Y's can also be determined from the radiative decay widths of the vector mesons and the two-gamma widths of the pseudoscalar mesons;[2,16] these constraints are shown in Fig. 11c and Fig. 11d.

Although both determinations agree on the quark content of the η, there seems to be a disagreement on the value of $|X_{\eta\prime}|$. However, each one of the three evaluations of $|X_{\eta\prime}|$—derived respectively from the $\eta\prime \to \gamma\rho^0$, $\eta\prime \to \gamma\omega^0$, and $\eta\prime \to \gamma\gamma$ partial widths—depends upon one number, $\Gamma(\eta\prime \to \gamma\gamma)$, which was used in the calculation of the $\eta\prime$ total width. Thus, if $\Gamma(\eta\prime \to \gamma\gamma)$ were to change by 30%, the results would agree. The usual 10° pseudoscalar mixing angle corresponds to $|X_{\eta\prime}| \simeq \frac{1}{\sqrt{2}}$, a value inconsistent with both the radiative transitions and these measurements. Unlike the η, the measured light quark content of the $\eta\prime$, 65%, is 2σ away from unity. This suggests that an additional component is present in the wave function of the $\eta\prime$ and supports models in which the η and $\eta\prime$ are mixed with a pseudoscalar glueball or radially excited quark-antiquark states.[2,12]

3.2 Electromagnetic Decays

We discuss the $\omega\pi^0$ channel which is electromagnetic and does not have the complications of the $\rho^0\eta$ channel, discussed above. This channel also has the best measured crossed channel amplitude, describing $\omega \to \gamma\pi^0$.

The electromagnetic current matrix element for the final state is given by

$$\langle \omega\pi^0 | J_\mu | 0 \rangle = f(q^2)\epsilon_{\mu\nu\sigma\rho} e_\omega^\nu P_\omega^\sigma P_\pi^\rho,$$

where $q^2 = m_{J/\psi}^2$; e_ω and $P_\omega(P_\pi)$ are the polarisation and four–momentum vectors of the $\omega(\pi)$, respectively. The electromagnetic $\omega\pi^0$ form factor at $q^2 = 0$ is deter-

mined by the $\omega \to \gamma\pi^0$ decay rate. Thus, using $\Gamma_{\mu^+\mu^-}$ to eliminate the coupling of the J/ψ to the intermediate photon, we can measure the ratio of form factors $|f(q^2 = m^2_{J/\psi})/f(q^2 = 0)|$:

$$\frac{|f(m^2_{J/\psi})|^2}{|f(0)|^2} = \frac{\alpha}{3}\left(\frac{k_\gamma}{P_\omega}\right)^3 \frac{m_{J/\psi}}{\Gamma_{\omega\to\pi\gamma}} \frac{\Gamma_{J/\psi\to\omega\pi}}{\Gamma_{J/\psi\to\mu\mu}}$$

where k_γ is the photon momentum in the ω rest frame and P_ω is the center of mass momentum in the $\omega\pi^0$ final state. Using our measured value for the branching ratio $B(J/\psi \to \omega\pi^0)$ and the Particle Data Group[11] values for $\Gamma_{J/\psi}$, Γ_ω, $m_{J/\psi}$, $B(J/\psi \to \mu^+\mu^-)$, and $B(\omega \to \gamma\pi^0)$, we obtain

$$\frac{|f(m^2_{J/\psi})|}{|f(0)|} = 0.038 \pm 0.006.$$

Note that this drop in the form factor from $q^2 = 0$ to $q^2 = m^2_{J/\psi}$ is about 2.5 times greater than the drop in the analogous $\pi\pi$ form factor measured in $J/\psi \to \pi^+\pi^-$.[6,17] This difference in energy dependence agrees qualitatively with the one expected from hadronic-helicity conservation.[18]

4. Acknowledgements

We would like to thank H.E. Haber and J.L. Rosner for helpful discussions. We gratefully acknowledge the dedicated support of SLAC's SPEAR and Linear Accelerator operating staff. We would also like to thank the technical and engineering staffs of group D at SLAC and the collaborating universities. One of us (N.W.) would like to thank the Alexander von Humboldt foundation for support.

Appendix

The different $J/\psi \to VP$ amplitudes are calculated from the effective interaction Lagrangian[19]

$$\mathcal{L} = G \cdot V^a P_a + E \cdot d_{abc} S^a V^b P^c$$

where V^a and P^a are the vector and pseudoscalar nonets, d_{abc} are the SU(3) structure constants, and S^a is a spurion field with the photon SU(3) transformation properties. G is the 3-gluon annihilation amplitude and E is the electromagnetic amplitude, proportional to the quark magnetic moment μ. The vector meson nonet is assumed ideally mixed.

The effect of the SU(3) breaking ($m_u = m_d \neq m_s$) on G is taken into account by the extra term

$$H \cdot d_{abc} S'^a V^b P^c$$

where S'^a transforms like the octet 8th component.

Since $\mu \propto 1/m$, the electromagnetic contribution to a specific channel has to be corrected when strange quarks are involved. The calculation is straightforward and results in different multiplicative functions of $x = \mu_s/\mu_u$ that are given in Table 3.

Finally, g, h and e are defined by

$$g = G + \frac{H}{\sqrt{3}}$$
$$h = \frac{\sqrt{3}}{2} H$$
$$e = \frac{E}{3}.$$

References

(a) Present Address: Physics Dept., Univ. of Utah, Salt Lake City, UT 84112, USA

(b) Present Address: CERN, EP, 1211 Geneva 23, Switzerland

(c) Present Address: SLAC, Stanford University, Stanford, CA 94305, USA

(d) Present Address: Applied Technology, Sunnyvale, CA 94086, USA

(e) Present Address: Anadrill/Schlumberger, Sugarland, Texas 77478, USA

(f) Present Address: ESL, Sunnyvale, CA 94088-3510, USA

(g) Present Address: Institute of High Energy Physics, Bejing, China

(h) Present Address: ORSAY, LAL, France

(i) Present Address: Lockheed Research, Palo Alto, CA 94302, USA

(j) Present Address: Phys. Dept., KEK Tsukuba, Ibaraki 305, Japan

(k) On leave of absence from Univ. of Pisa, Pisa, Italy

(l) Present Address: Physics Dept., Northeastern Univ., Boston, MA 02115, USA

1. E.D. Bloom, *Proc. SLAC Summer Inst. on Part. Phys.*, **SLAC-REP 245**, (1982) and references quoted therein.

2. See, for example:
   H.J. Lipkin, *Phys. Lett.* **67B**, 65 (1977).
   J.L. Rosner, private communication. See also *Phys. Rev.* **D27**, 1101 (1983) and references 4–15 quoted therein.

3. S. Okubo, *Phys. Rev.* **D13**, 1994 (1976).
   H. Kowalski and T.F. Walsh, *Phys. Rev.* **D14**, 852 (1976).
   S. Rudaz, *Phys. Rev.* **D14**, 298 (1976).

4. D. Bernstein et al., *Nucl. Instr. Methods.* **226**, 301 (1984).

5. P.A. Carruthers, *"Spin and Isospin in Particle Physics"*, edited by Gordon and Breach, New York (1971).

6. R.M. Baltrusaitis et al., *SLAC-PUB-3562*, submitted to *Phys. Rev. D*

7. For a detailed discussion, see J.D. Richman, Ph.D. Thesis, California Institute of Technology, *CALT-68-1231*, (1985)(unpublished)

8. For a detailed discussion, see A.L. Spadafora, Ph.D. Thesis, Illinois Univ., *COO-1195-495*, (1984)(unpublished)

9. S. Okubo, *Phys. Lett.* **5**, 165 (1963)
G.Zweig, 1964 (unpublished)
J. Iizuka, *Prog. Theor. Phys. Suppl.* **37-38**, 21 (1966).

10. J.D. Jackson, *Nuovo Cimento*, **XXXIV**, 1644 (1964).

11. Particle Data Group, *Rev. Mod. Phys.* **56**, No. 2 part II (1984).

12. A different analysis can be found in:
S. Pinsky, *Phys. Rev.* **D31**, 1753 (1985).

13. See, for example:
W. Palmer, S. Pinsky, and C. Bender, *Phys. Rev.* **D30**, 1002 (1984).
E. Kawai, *Phys. Lett.* **124B**, 262 (1983).
C.E. Carlson and T.H. Hansson, *Nucl. Phys.* **B199**, 441 (1982).
S. Iwao, *Nuov. Cim. Lett.* **35**, 209 (1982).
C. Rosenzweig, *proceeding of the MRST meeting*, **1**, (1982).
K. Senba and M. Tanimoto, *Nuov. Cim. Lett.* **35**, 295 (1982).

14. A possible difference between the pseudoscalar form factors or other corrections to the first order theory have not been taken into account.

15. A. De Rújula, H. Georgi and S.L. Glashow, *Phys. Rev.* **D12**, 147 (1975).

16. We used the following partial width values:

- $\Gamma(\omega \to \gamma\pi^0) = (861 \pm 56)$ keV, $\Gamma(\phi \to \gamma\eta) = (50.6 \pm 8.6)$ keV, $\Gamma(\pi^0 \to \gamma\gamma) = (7.8 \pm 0.6)$ eV and $\Gamma(\eta \to \gamma\gamma) = (343 \pm 47)$ eV; from Ref. 11.

- $\Gamma(\rho^0 \to \gamma\eta) = (55 \pm 14)$ keV and (83 ± 17) keV, the two possible solutions obtained by D. Andrews et. al., *Phys. Rev. Lett.* **38**, 198 (1977).

- $\Gamma(\eta\prime \to \gamma\gamma) = (4.16 \pm 0.43)$ keV, average of the results obtained by the PLUTO (*Phys. Lett.* **142B**, 125 (1984)) and TASSO (*Phys. Lett.* **147B**, 487 (1984)) collaborations.

- $\Gamma(\eta\prime \to \gamma\rho^0) = (66 \pm 10)$ keV and $\Gamma(\eta\prime \to \gamma\omega) = (6.1 \pm 1.4)$ keV were calculated from the known $\eta\prime$ branching ratios and its total width, (219 ± 32) keV, which was derived from $\Gamma(\eta\prime \to \gamma\gamma)$ and $B(\eta\prime \to \gamma\gamma)$.

17. W. Braunschweig et al., *Phys. Lett.* **63B**,487 (1976).
F. Vannucci et al., *Phys. Rev.* **D15**, 1814 (1977).
R. Brandelik et al., *Z. Phys.* **C1**, 233 (1979).

18. S.J. Brodsky and G.P. Lepage, *Phys. Rev.* **D24**, 2848 (1981)

19. H. Kowalski and T.F. Walsh, *Phys. Rev.* **D14**, 852 (1976).
P.J. O'Donnell, *Rev. Mod. Phys.* **53**, 673 (1981).
N. Isgur, *Phys. Rev. Lett.* **36**, 1262 (1976).

Table 1: $J/\psi \to VP$ Branching Ratios.

Unless specified, the π^0 and η in the final state are identified by their $\gamma\gamma$ decay and the K_S by its $\pi^+\pi^-$ decay mode. The first error is statistical and the second one is systematic. The upper limits are given at the 90% confidence level.

Decay Mode	Final State	Branching Ratio in unit of 10^{-3}
$\rho\pi$	$\pi^0\pi^+\pi^-$	$13.3 \pm 0.3 \pm 1.5$
$K^{*+}K^- + c.c.$	$K^\pm\pi^\mp K_S$	$5.0 \pm 0.25 \pm 0.6$
	$K^+K^-\pi^0$	$6.0 \pm 0.3 \pm 0.7$
$K^{*0}\bar{K}^0 + c.c.$	$K^\pm\pi^\mp K_S$	$3.9 \pm 0.2 \pm 0.6$
$\omega\eta$	$\pi^0\pi^+\pi^-\eta$	$1.9 \pm 0.2 \pm 0.3$
$\omega\eta\prime$	$\pi^0\pi^+\pi^-\gamma\rho^0$	$0.39 \pm 0.11 \pm 0.06$
	$\pi^0\pi^+\pi^-\eta\pi^+\pi^-$	$0.43^{+0.19}_{-0.22} \pm 0.07$
$\phi\eta$	$K^+K^-neutrals$	$0.69 \pm 0.07 \pm 0.08$
	$K^+K^-\eta$	$0.64 \pm 0.15 \pm 0.08$
	$K^+K^-\pi^0\pi^+\pi^-$	$0.61 \pm 0.14 \pm 0.08$
$\phi\eta\prime$	$K^+K^-\gamma\rho^0$	$0.39 \pm 0.10 \pm 0.06$
	$K^+K^-\eta\pi^+\pi^-$	$0.365 \pm 0.04 \pm 0.05$
$\omega\pi^0$	$\pi^0\pi^+\pi^-\pi^0$	$0.67 \pm 0.06 \pm 0.11$
$\rho^0\eta$	$\pi^+\pi^-\eta$	$0.18 \pm 0.02 \pm 0.04$
$\rho^0\eta\prime$	$\pi^+\pi^-\eta\pi^+\pi^-$	< 0.1
$\phi\pi^0$	$K^+K^-\pi^0$	< 0.013

Table 2: $J/\psi \to \eta\pi^+\pi^-$.

Results of fits to the $\pi^+\pi^-$ effective mass distribution.
The χ^2 per degree of freedom of each fit is equal to 35/27.

Fit 1	Fit 2
$N_\omega = 5.0 \pm 2.4$	$N_\omega = 8.9$; fixed
$N_{\rho^0} = 58.5 \pm 7.4$	$N_{\rho^0} = 49.5 \pm 6.3$
$\phi = 0.4 \pm 0.5$	$\phi = 0.4 \pm 0.5$

Table 3: $J/\psi \to VP$ amplitudes.

Decay Mode	Amplitude
$\rho^+\pi^-;\rho^0\pi^0;\rho^-\pi^+$	$g \quad +e$
$K^{*+}K^-;K^{*-}K^+$	$g \quad -h+e\cdot(2-x)$
$K^{*0}\bar{K}^0;\bar{K}^{*0}K^0$	$g \quad -h-2e\cdot(\frac{1+x}{2})$
$\omega\eta$	$(g \quad +e)X_\eta$
$\omega\eta\prime$	$(g \quad +e)X_{\eta\prime}$
$\phi\eta$	$(g-2h-2e\cdot x)Y_\eta$
$\phi\eta\prime$	$(g-2h-2e\cdot x)Y_{\eta\prime}$
$\rho^0\eta$	$3eX_\eta$
$\rho^0\eta\prime$	$3eX_{\eta\prime}$
$\omega\pi^0$	$3e$
$\phi\pi^0$	0

Table 4: Quark Content of the η and $\eta\prime$ determined from ratios of decay rates.

Ratio	Coefficient
$\frac{\omega\eta}{\rho^0\pi^0}$	$X_\eta^2 = 0.48 \pm 0.10$
$\frac{\rho^0\eta}{\omega\pi^0}$	$X_\eta^2 = 0.29 \pm 0.09$
$\frac{\omega\eta\prime}{\rho^0\pi^0}$	$X_{\eta\prime}^2 = 0.13 \pm 0.04$
$\frac{\rho^0\eta\prime}{\omega\pi^0}$	$X_{\eta\prime}^2 < 0.21$ (90% C.L.)
$\frac{\phi\eta\prime}{\phi\eta}$	$\frac{Y_{\eta\prime}^2}{Y_\eta^2} = 0.76 \pm 0.14$

Table 5: Results of the Global Fit

$\|g\| = 1.17 \pm 0.06$	$\|X_\eta\| = 0.63 \pm 0.06$
$\|h\| = 0.24 \pm 0.07$	$\|Y_\eta\| = 0.83 \pm 0.13$
$\|e\| = 0.15 \pm 0.01$	$\|X_{\eta'}\| = 0.36 \pm 0.05$
$\phi = 1.19 \pm 0.20$	$\|Y_{\eta'}\| = 0.72 \pm 0.12$

Figure Captions

1. (a) Three gluon annihilation. (b) Electromagnetic decay proceeding via $c\bar{c}$ annihilation into one photon. (c) Radiative decay into a final state of one photon and two gluons. (d) Magnetic dipole radiative transition to the $\eta_c(2980)$.

2. The MARK III detector (a) View transverse to the beam axis. (b) Parallel.

3. Dalitz plots for (a) $J/\psi \to \pi^+\pi^-\pi^0$. (b) $J/\psi \to K^+K^-\pi^0$. (c) $J/\psi \to K^{\pm}\pi^{\mp}K^0_S$ events.

4. (a) The $\gamma\gamma$ momentum spectrum for $J/\psi \to \gamma\gamma\omega$, $\omega \to \pi^+\pi^-\pi^0$ events. The peak at 1.44 GeV/c is from $J/\psi \to \omega\pi^0$, while the one at 1.40 GeV/c is from $J/\psi \to \omega\eta$. (b) Invariant $\gamma\gamma$ mass spectrum recoiling against the ω.

5. Distribution of $\cos\theta_1$, where θ_1 is the angle in the ω rest frame between the ω direction and the normal to the decay plane (a) $J/\psi \to \omega\pi^0$. (b) $J/\psi \to \omega\eta$. The curves are the result of a fit to a second order polynomial which yields coefficients in very good agreement with $(1 - cos^2\theta)$.

6. The $\gamma\gamma$ mass plot for the two gammas recoiling against the ϕ for $J/\psi \to \gamma\gamma\phi$ events.

7. (a) The K^+K^- invariant mass for four prong events. (b) The $\pi^+\pi^-$ invariant mass versus the $\gamma\pi^+\pi^-$ mass, for events of the type $J/\psi \to \gamma\pi^+\pi^-\phi$, $\phi \to K^+K^-$. (c) The $\gamma\gamma$ invariant mass versus the $\gamma\gamma\pi^+\pi^-$ mass, for events of the type $J/\psi \to \gamma\gamma\pi^+\pi^-\phi$, $\phi \to K^+K^-$.

8. (a) The $\gamma\pi^+\pi^-$ invariant mass recoiling against the ω for events of the type $J/\psi \to \gamma\pi^+\pi^-\omega$, $\omega \to \pi^0\pi^+\pi^-$. (b) The $\eta\pi^+\pi^-$ invariant mass recoiling against the ω for events of the type $J/\psi \to \eta\pi^+\pi^-\omega$, $\omega \to \pi^0\pi^+\pi^-$.

9. The $\pi^+\pi^-$ invariant mass for events of the type $J/\psi \to \pi^+\pi^-\eta$. The curves represent (a) $|A_{\rho 0} + A_\omega|^2$ + background. (b) $|A_{\rho 0}|^2$ + background. (c) $|A_\omega|^2$ + background. (d) background (See text).

10. (a) Doubly disconnected diagram. (b) Singly disconnected diagram.

11. Constraints on X and Y: (a) and (b) from $J/\psi \to VP$ decays (c) and (d) from radiative transitions. The shaded line in Part b corresponds to the 90% confidence level upper limit on $X_{\eta\prime}$ given in Table 4. In Part c, the two vertical bands correspond to the two possible solutions for $\Gamma(\rho^0 \to \gamma\eta)$ (see Ref. 15). $\eta_1(\eta_8)$ shows the quark content expected for a pure singlet $\eta\prime$ (octet η). The 10° pseudoscalar mixing angle predictions are also shown.

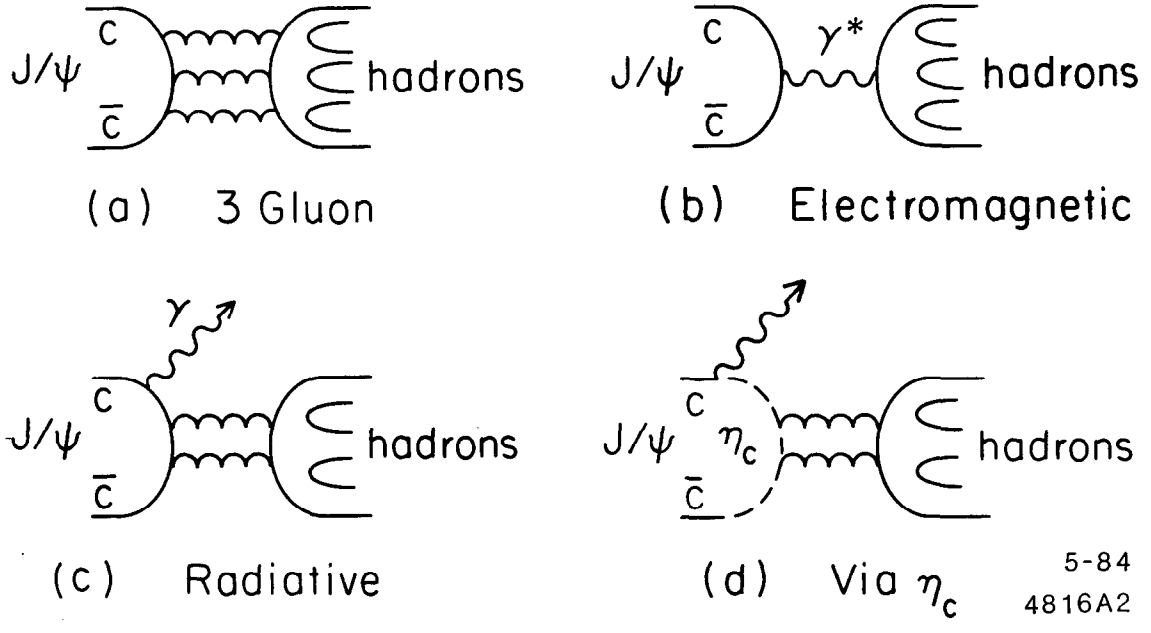
J/ψ
c
c̄
hadrons
(a) 3 Gluon
γ*
(b) Electromagnetic
γ
(c) Radiative
ηc
(d) Via ηc
5-84
4816A2

Fig. 1

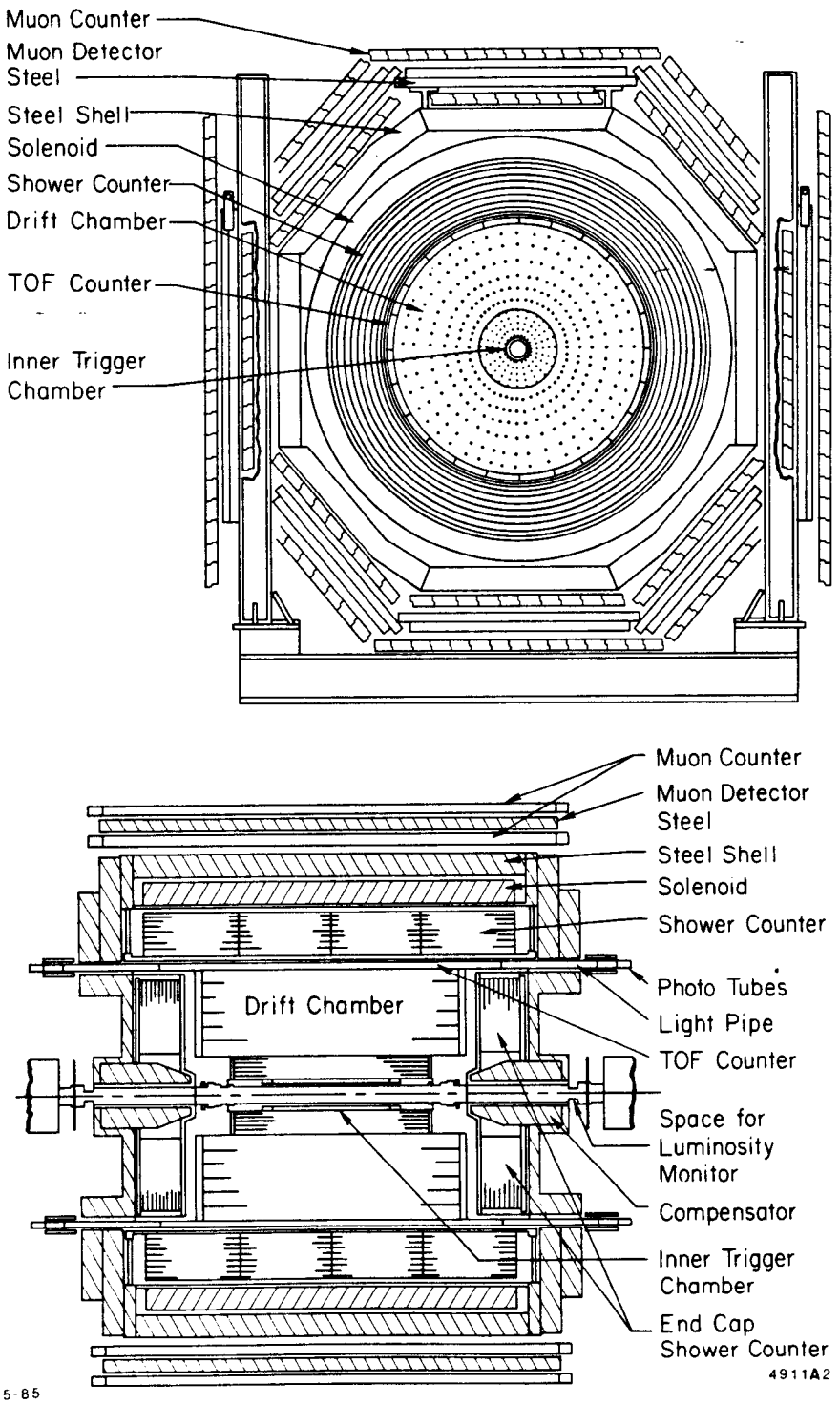
Muon Counter
Muon Detector Steel
Steel Shell
Solenoid
Shower Counter
Drift Chamber
TOF Counter
Inner Trigger Chamber
Muon Counter
Muon Detector Steel
Steel Shell
Solenoid
Shower Counter
Photo Tubes
Light Pipe
TOF Counter
Drift Chamber
Space for Luminosity Monitor
Compensator
Inner Trigger Chamber
End Cap Shower Counter
4911A2
5-85

Fig. 2

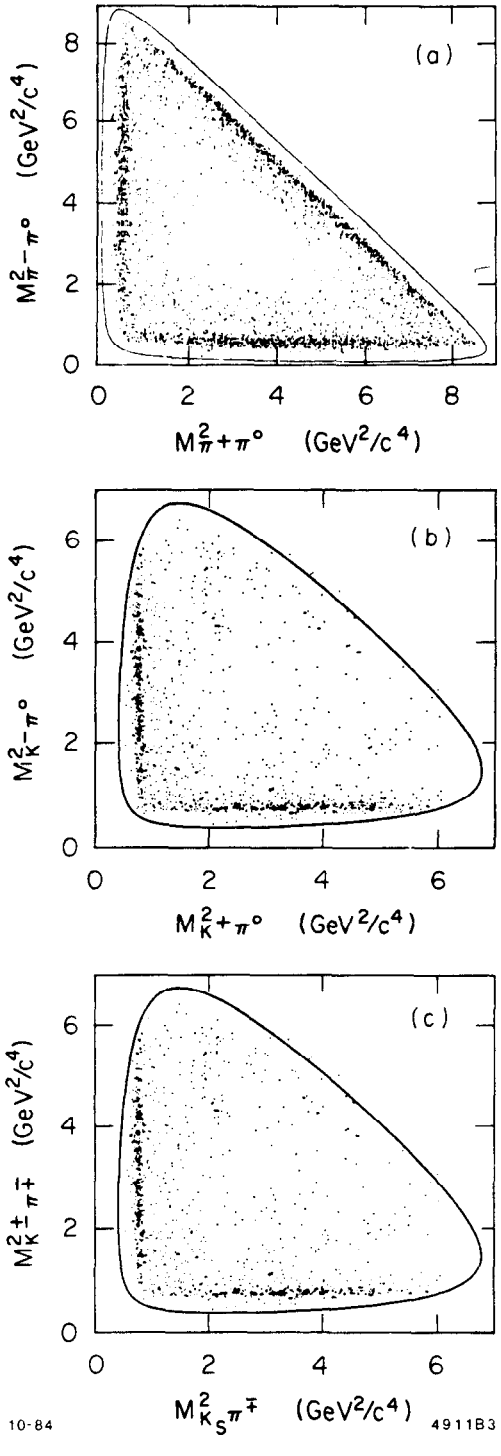
(a)
$M^2_{\pi^-\pi^0}$ (GeV^2/c^4)
$M^2_{\pi^+\pi^0}$ (GeV^2/c^4)
(b)
$M^2_{K^-\pi^0}$ (GeV^2/c^4)
$M^2_{K^+\pi^0}$ (GeV^2/c^4)
(c)
$M^2_{K^\pm\pi^\mp}$ (GeV^2/c^4)
$M^2_{K_S\pi^\mp}$ (GeV^2/c^4)
10-84
4911B3

Fig. 3

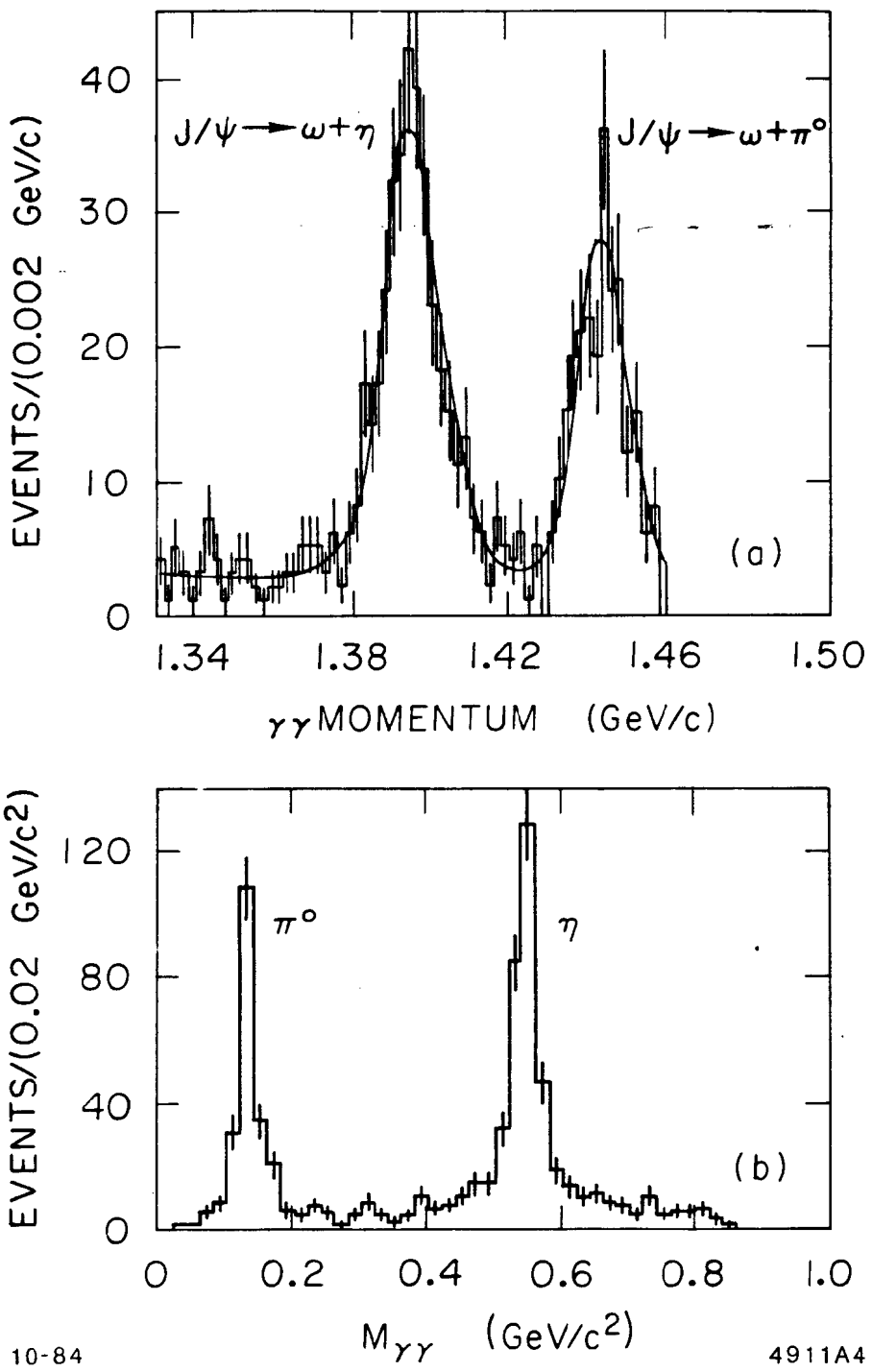
EVENTS/(0.002 GeV/c)
40
30
20
10
0
J/ψ → ω+η
J/ψ → ω+π°
(a)
1.34
1.38
1.42
1.46
1.50
γγ MOMENTUM (GeV/c)
EVENTS/(0.02 GeV/c²)
120
80
40
0
π°
η
(b)
0
0.2
0.4
0.6
0.8
1.0
Mγγ (GeV/c²)
10-84
4911A4

Fig. 4

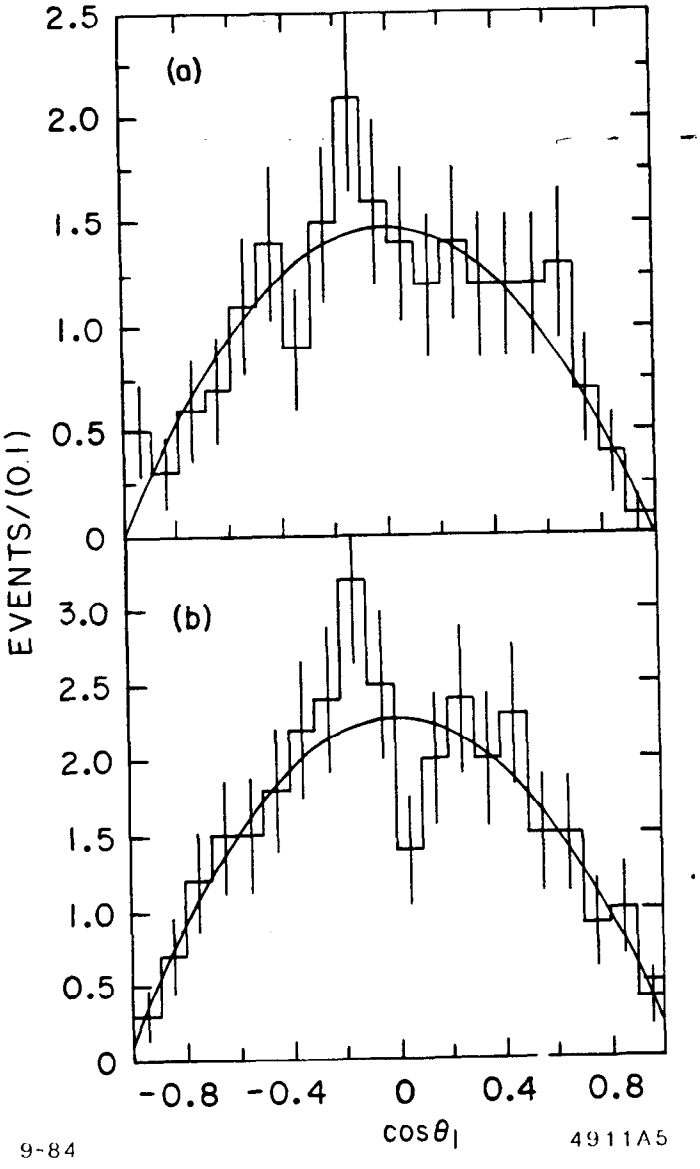
(a)
(b)
EVENTS/(0.1)
2.5
2.0
1.5
1.0
0.5
0
3.0
2.5
2.0
1.5
1.0
0.5
0
-0.8
-0.4
0
0.4
0.8
cosθl
9-84
4911A5

Fig. 5

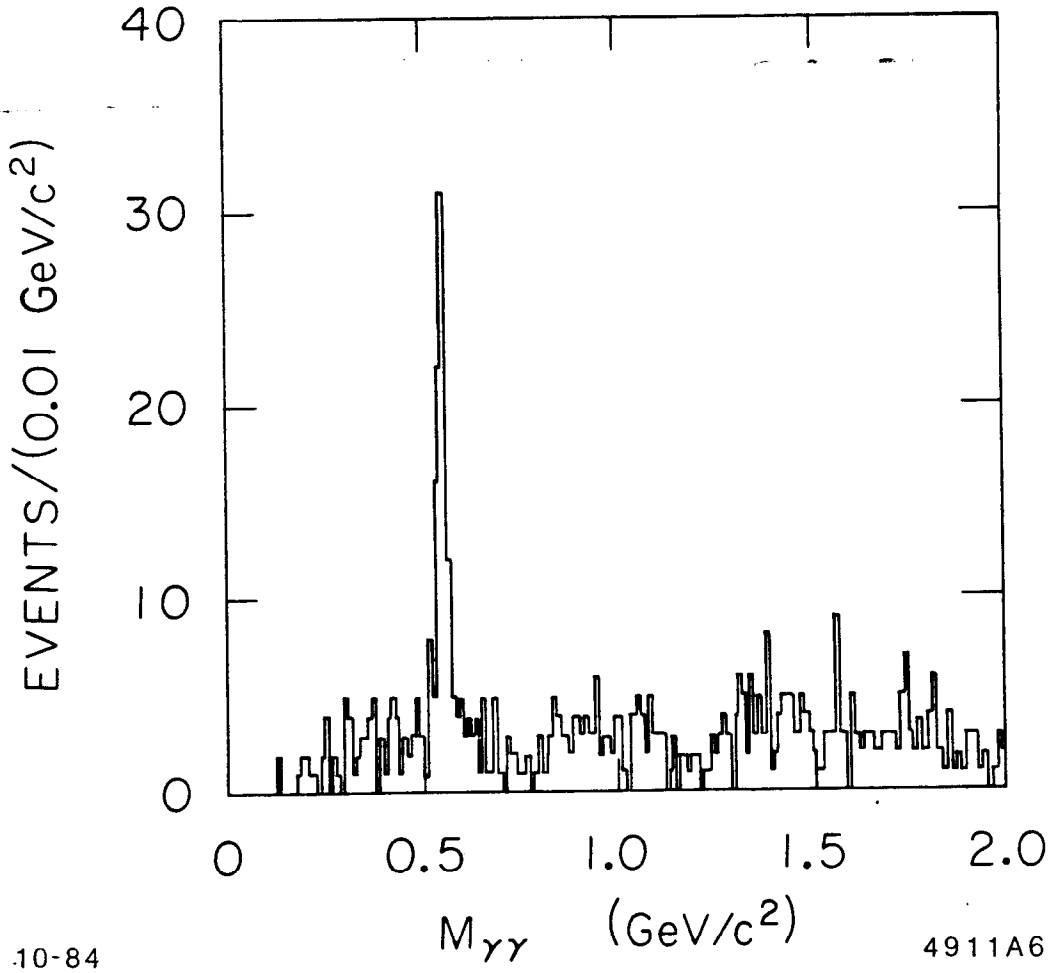
40
30
20
10
0
EVENTS/(0.01 GeV/c²)
0
0.5
1.0
1.5
2.0
Mγγ (GeV/c²)
10-84
4911A6

Fig. 6

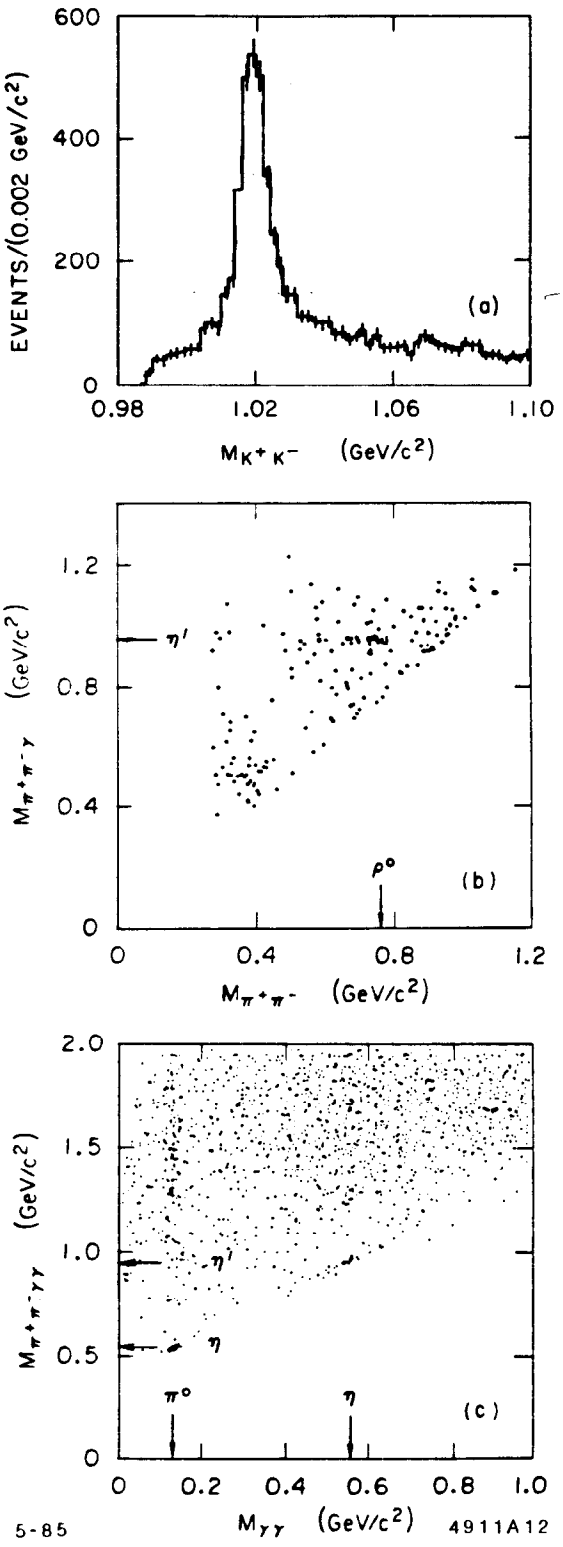
EVENTS/(0.002 GeV/c²)
600
400
200
0
0.98
1.02
1.06
1.10
(a)
M_K⁺K⁻ (GeV/c²)
M_π⁺π⁻γ (GeV/c²)
1.2
0.8
0.4
0
η'
ρ°
(b)
0
0.4
0.8
1.2
M_π⁺π⁻ (GeV/c²)
M_π⁺π⁻γγ (GeV/c²)
2.0
1.5
1.0
0.5
0
η'
η
π°
η
(c)
0
0.2
0.4
0.6
0.8
1.0
M_γγ (GeV/c²)
5-85
4911A12

Fig. 7

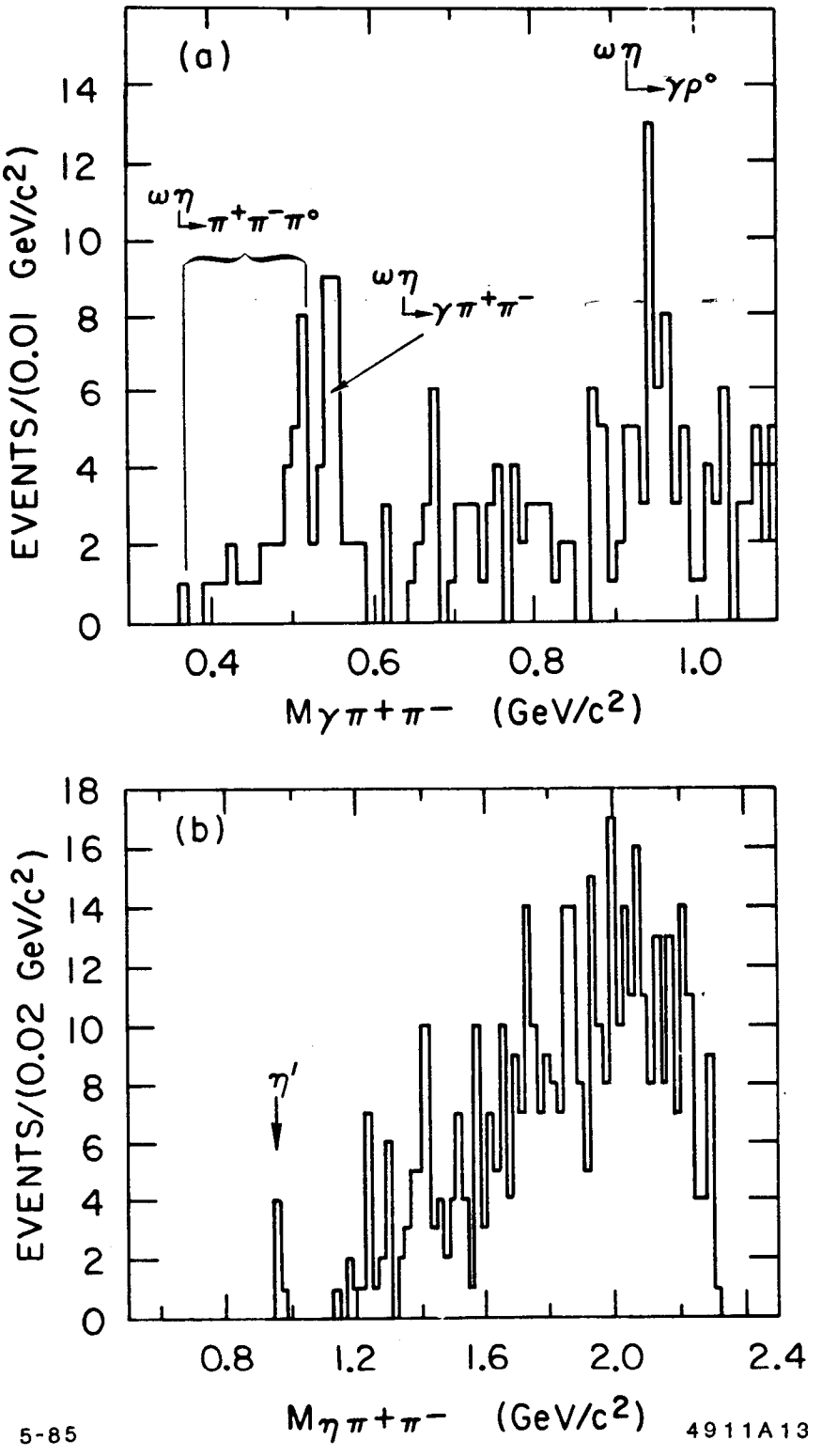
(a)
ωη
→γρ°
ωη
→π+π−π°
ωη
→γπ+π−
EVENTS/(0.01 GeV/c²)
0
2
4
6
8
10
12
14
0.4
0.6
0.8
1.0
Mγπ+π− (GeV/c²)
(b)
η′
EVENTS/(0.02 GeV/c²)
0
2
4
6
8
10
12
14
16
18
0.8
1.2
1.6
2.0
2.4
Mηπ+π− (GeV/c²)
5-85
4911A13

Fig. 8

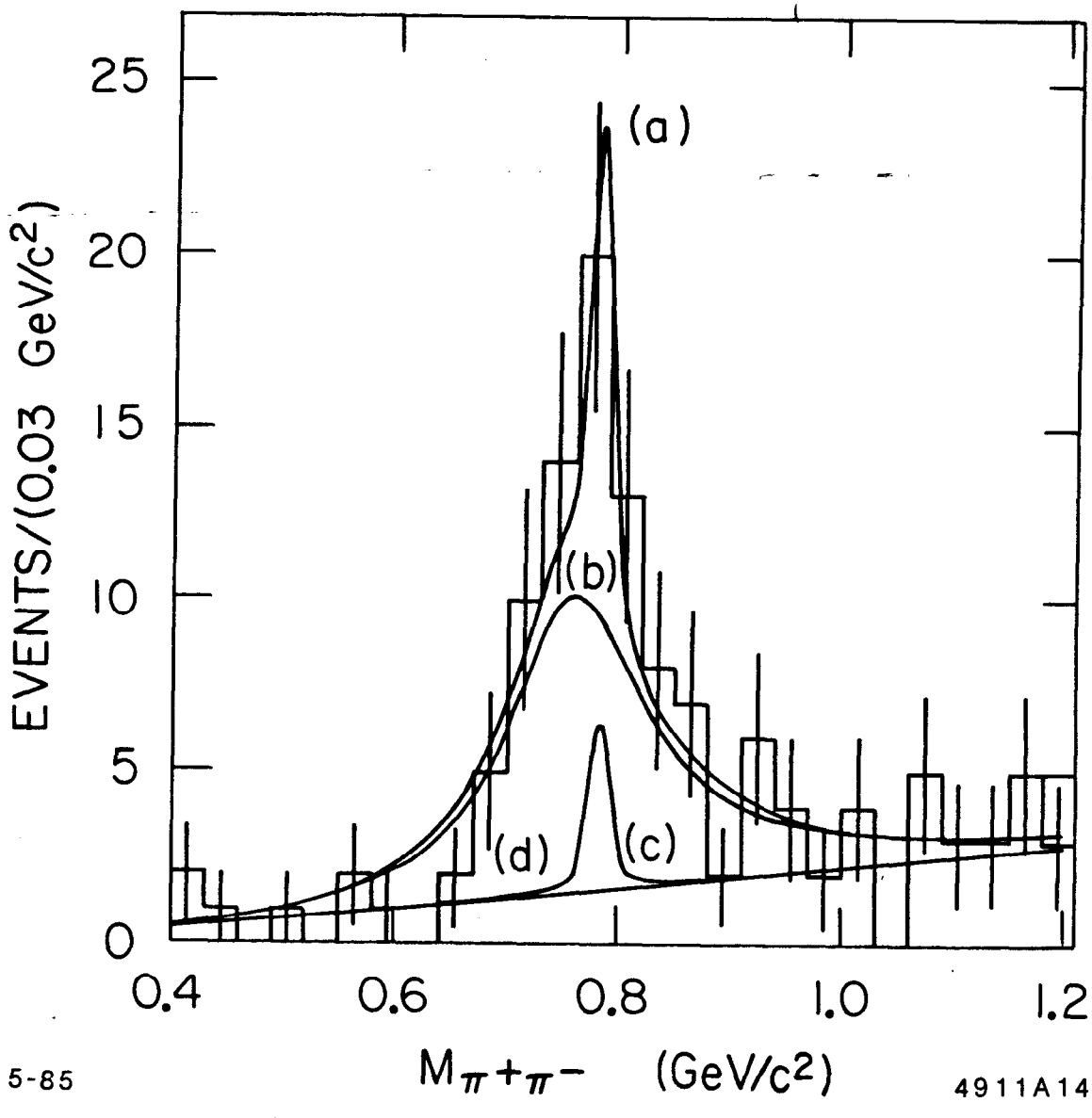
25
20
15
10
5
0
EVENTS/(0.03 GeV/c²)
(a)
(b)
(c)
(d)
0.4
0.6
0.8
1.0
1.2
Mπ+π− (GeV/c²)
5-85
4911A14

Fig. 9

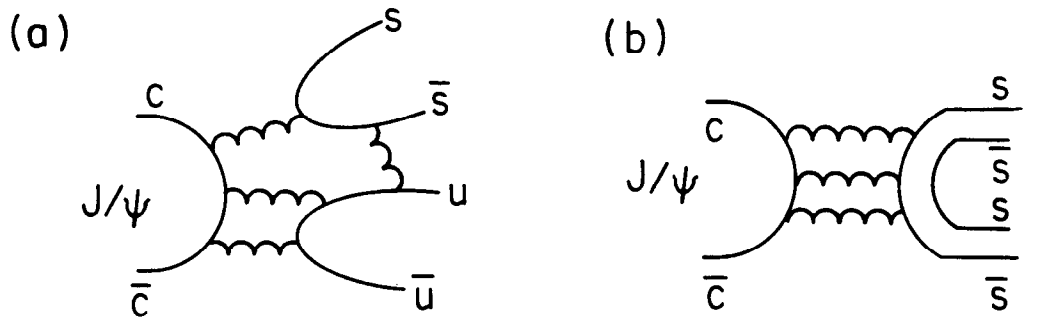

Fig. 10

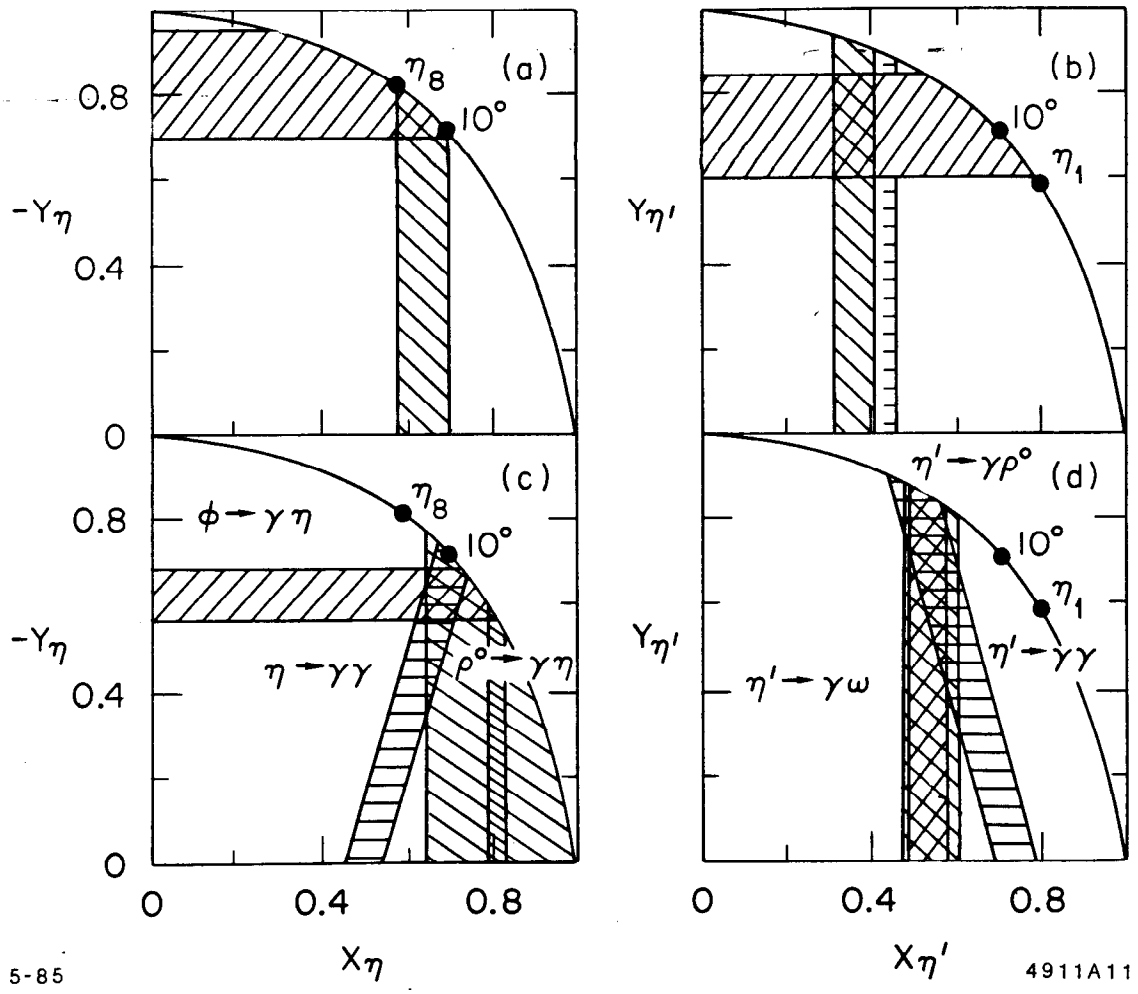
(a)
(b)
(c)
(d)
η_8
η_1
10°
$-Y_\eta$
$Y_{\eta'}$
0.8
0.4
0
$\phi \to \gamma\eta$
$\eta \to \gamma\gamma$
$\rho^\circ \to \gamma\eta$
$\eta' \to \gamma\rho^\circ$
$\eta' \to \gamma\omega$
$\eta' \to \gamma\gamma$
X_η
$X_{\eta'}$
5-85
4911A11

Fig. 11